Femtosecond, Frequency-Agile, Phase-Sensitive-Detected, Multi-Wave-Mixing Nonlinear Optical Spectroscopy Applied to π-Electron Photonic Materials

K. A. Drenser, R. J. Larsen, F. P. Strohkendl, and L. R. Dalton*

Loker Hydrocarbon Research Institute, University of Southern California, California 90089-1662, and Department of Chemistry, University of Washington, Seattle, Washington 98195-1700

Received: September 9, 1998; In Final Form: December 9, 1998

Degenerate four-wave mixing (DFWM) spectroscopy is modified to exploit femtosecond pulses, phase-sensitive-detection, frequency (wavelength) agility, two-color (nearly degenerate multiwave mixing) radiation, and improved signal-to-noise capabilities that can be realized through a combination of new solid state lasers, nonlinear optical components, and novel design concepts. The resulting time-resolved nonlinear optical techniques permit "instantaneous" optical nonlinearities, such as two-photon absorption cross sections, to be accurately measured over the spectral range from 450 to 2500 nm (and with significantly greater effort from 225 to 5000 nm). The power of the new techniques is illustrated by their application to the definition of H_g two-photon resonances of C_{60} and C_{70} as well as to the characterization of optical nonlinearities in two linear chromophores of putative utility for sensor protection and electrooptic modulation. Explicitly, these measurements provide accurate determination of both transition energies and transition moments (matrix elements connecting the two photon levels). Results are compared to those previously reported in the literature illustrating the advantages and problems associated with particular measurement techniques. All of the molecules studied are found to exhibit two-photon absorption coefficients comparable to that of GaAs, the most studied putative sensor protection material (based on utilization of electronic optical nonlinearity). Femtosecond pulse techniques are shown, in all cases, to be necessary to avoid complications arising from excited-state absorption and relaxation phenomena. The importance of phase-sensitive detection in identifying complications from overlapping transitions is illustrated.

Introduction

The pioneering spectroscopic studies of Kohler[1] on polyenes and other π-electron molecules established the importance of the competition of electron−phonon and electron Coulomb interactions in defining the relative positions of one- and two-photon-allowed excited states in delocalized π-electron materials. Such data, collected largely through gas-phase studies, provided critical tests of quantum mechanical calculations attempting to predict the electronic properties of quasi-delocalized electron systems. In particular, molecular orbital theories at the single configuration level were shown to be inadequate for predicting the relative positions of the $2\ ^1A_g$ and ^1B_u levels and vibronic coupling between the $1\ ^1A_g$ and $2\ ^1A_g$ states was shown to be important in defining the position of the $2\ ^1A_g$ state for polyenes.[1]

The defining of the electronic structures of molecules, macromolecules, and polymers with extended π-electron systems has taken on a new importance over the past two decades as these materials have been considered for potential technologically important applications of sensor protection, all-optical information processing, electrooptic modulation, photorefraction, and electroluminescence.[2] Moreover, π-electron materials play a central role in biologically based optical to electrical energy transduction processes critical to phenomena ranging from vision to photosynthesis. Biomolecules, such as bacteriorhodopsin, may in turn have technological utility, e.g., for high-density optical memories.[3] As the aforementioned device applications and biological phenomena typically involve condensed matter materials, spectroscopic investigations were broadened to include extensive studies of liquid and solid state samples. In turn, as device performance is strongly influence by excited-state absorption and relaxation processes, spectroscopic studies had to be extended to include characterization of temporal effects (e.g., dependence of measured phenomena upon pulse width and evolution of the system following pulsed excitation). The demand for more extensive characterization of the electronic properties of π-electron materials has resulted in a wide range of nonlinear spectroscopic tools being used to study these materials, including third-harmonic generation (THG), degenerate four-wave mixing (DFWM), dynamic Kerr effect (DKE), pump−probe (PP), electric, field-induced second-harmonic (EFISH) generation, Z-scan, and electroabsorption (EA).[4] As more techniques have been brought to bear and correlation of data from different techniques attempted, the issue of the influence of measurement conditions upon the characterization of nonlinear optical properties has come to the forefront. In particular, the role of pulse conditions is of ever increasing concern.

In this article, we discuss the development and application of new spectroscopic techniques that permit improved definition of the position and absorption cross-section of two-photon excitations and permit a high-resolution characterization of electronic properties relevant to various technological applications. These techniques permit critical insight to be gained concerning the role of pulse width and pulse intensity in influencing experimental measurement of nonlinear optical parameters. The studies reported also emphasize the importance of phase-sensitive detection in assigning transition energies and in detecting complications that are signatures of overlapping transitions. Our discussion provides some insight into the current

10.1021/jp983651e CCC: $18.00
Published on Web 02/13/1999

status of sensor protection, all-optical information processing, and electrooptic modulation based on the use of π-electron organic materials. This is appropriate as all of the materials studied are under consideration for technological application based on their nonlinear optical properties.

While the focus of this article is largely upon the measurement of "instantaneous" optical nonlinearity using femtosecond pulses, we have also carried out detailed studies of the temporal response over different time domains using the analysis approach discussed in an earlier article published in this journal.[5] Because of space limitations, we defer discussion (with the exception of commenting on the complications to the analysis of two photon absorption coefficients arising from excited state absorption and relaxation) of extended time domain measurements to another article. In like manner, we will discuss each of the materials at a level consistent with published theoretical and experimental data. Thus, the highly studied fullerenes will be analyzed in greater detail and particular attention will be given not only to discussion of the magnitude of two-photon absorption but also the assignment of the lowest lying two-photon state. However, the comparison of magnitudes of two photon absorption for the four π-electron molecules studied here and the comparison of these with the two photon absorption of GaAs is interesting both from scientific and technological viewpoints. Let us begin our discussion with a brief literature review of the highly studied C_{60} system as this illustrates the difficulties of assigning two photon transition energies and characterization of absorption coefficients.

C_{60}: Linear and Nonlinear Optical Properties. Historical Perspective

An evaporated thin film of C_{60} is an amorphous van der Waals solid, where the molecules rotate freely at ambient temperatures. Optical[6] and photoemission[7] measurements suggest that the electronic structure of C_{60} molecules is very similar in gaseous and condensed phases consistent with free rotation. The ground electronic state is a singlet of A_g symmetry and the lowest lying excited state is a triplet 1.55 eV above the ground state.[8] The first excited state accessible by a one-photon electric-dipole-allowed transition is near 3.3 eV, and theory attributes this excitation to an excited state of T_{1u} symmetry.[9,10] Various theories do not agree on the energy of this and other excited states but they do agree on existence of at least a half dozen singlet levels below the T_{1u} level. These levels are of symmetries T_{1g}, T_{2g}, G_g, G_u, T_{2u}, H_u, and H_g. There are also a number of triplet states lying below the T_{1u} level. All theories agree that, of all the singlet states lying below the T_{1u} level, only the H_g state has a nonvanishing matrix element with the ground electronic state; this level can be excited by two-photon absorption (TPA). Theories disagree substantially on the exact position of this level and upon the magnitude of the two-photon absorption coefficient associated with the level. Also of significant theoretical interest is the position of the lowest energy two-photon A_g state lying above the T_{1u} state. Laszlo and Udvardi[10] predict the excitation energy of the lowest excited A_g state at 7.1 eV, somewhat below their value for $2E_g = 8.0$ eV (where E_g is the optical gap). Of all the excited state symmetries, only A_g reflects the full symmetry of the C_{60} ground state. Thus, we expect that an excitation of this kind to be a collective excitation of a large number of electrons which should give rise to a correspondingly large optical nonlinearity. Laszlo and Udvardi also predict five H_g states below 2 E_g with the lowest lying near 3.1 eV.

Nonlinear Optical Spectroscopic Measurements. Historical Perspective with Emphasis of C_{60} Measurements

The theoretical work described above clearly establishes the importance of identifying and defining the lowest lying two photon state of C_{60}. Third-harmonic generation (THG) measurements have suggested that two photon absorption to the lowest lying H_g state is centered at 1.3 ± 0.1 μm.[11] THG has traditionally been the method of choice for the exploration of purely electronic third-order optical nonlinearity and the electronic structure which gives rise to it. The large frequency shift between the input and signal beams in THG ensures that the signal is independent of laser pulse width and excited-state absorption. Unfortunately, as has been noted by Strohkendl et al.,[12] THG suffers from the unpredictable overlap of predictable three photon resonances with two photon resonances. Denoting the optical band gap as E_g, one finds that THG is able to detect two-photon absorption free of interference from one- and three-photon resonances only for excited-state energies up to $^2/_3E_g$. Because of the potential for inaccurate assignment of two-photon resonances using THG due to overlap with three-photon resonances, it is important to define the resonance frequency of two-photon transitions by other techniques.

DFWM can detect two-photon states without interference from other absorptions up to $2E_g$ which is a greater "free spectral range" than either THG or EA (which can detect TPA up to E_g). We have previously[5] demonstrated that DFWM is an effective means of investigating electronic relaxation and nuclear movement (e.g., structural relaxation of excitons, solitons, polarons, and bipolarons). However, the sensitivity of DFWM to all electronic and nuclear (including photoacoustic and thermal diffusion[13]) dynamics can be a liability in the measurement of two-photon absorption. Indeed, for nanosecond pulses, DFWM signals are typically dominated by thermal effects and are consequently unrelated to the electronic third-order optical nonlinearity. For DFWM to be useful for the characterization of instantaneous optical nonlinearity, four modifications of traditional DFWM are required: (1) utilization of femtosecond (100 fs or less) pulses to minimize excited-state absorption, (2) implementation of phase-sensitive-detection to separate two-photon absorption from nonlinear refractive index contributions (i.e., to separate imaginary and real components of the third-order nonlinear optical susceptibility), (3) measurement of the nonlinear optical spectra over a significant range of wavelengths to permit the line shape of excitations (e.g., two photon) to be determined and to permit deconvolution of various resonances through spectral simulation, and (4) improvement of laser pulse-to-pulse stability for the realization of good signal-to-noise. In previous publications,[12,14] we have discussed the implementation of these features and have demonstrated the existence of a two-photon absorption for C_{60} centered at an excitation wavelength of 0.93 μm (2.7 eV above the ground state). This is the only two-photon state detected for C_{60} in the spectral range 0.7 to 2.0 μm. The magnitude and phase of the DFWM coefficients are well fit by a Lorentzian model for a single resonance over this entire spectral range. More recent results from direct two-photon absorption measurements[15] clearly confirm our results.

Phase-sensitive-detection (PSD) was accomplished using the "signal lattice" concept illustrated in Figure 1. This technique derives from the fact that signal beams in DFWM depend on both sample and sample holder (e.g., substrate) materials. Three input laser beams denoted 1, 2, and 3 generate nine DFWM signal beams. Only one signal beam, denoted A, is phase-matched. This phase-matched signal involves thin-film (sample)

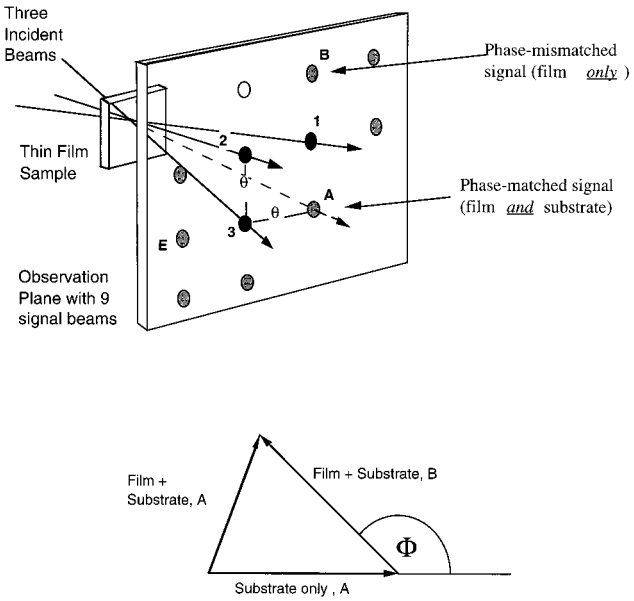

Figure 1. The geometry for phase-mismatched degenerate-four-wave mixing is shown. Three input beams generate nine signal beams. The phase-matched signal at point A arises from a superposition of the sample (e.g., thin film or solution) and sample holder (substrate or solution sample cell) signals. The remaining eight signals are all phase-mismatched and arise essentially from the thin sample. The inset shows the phasor diagram for the addition of the signal-field amplitudes in the phase-matched direction when all beam polarizations are parallel.

and thick-substrate (sample holder) contributions while the phase-mismatched signals arise essentially only from the thin film sample. The phase-matched signal is of the form $|E_s + E_f e^{i\phi}|^2$, while the phase-mismatched signals are of the form $|E_f|^2$; where E_s is the electric field amplitude of the substrate signal, E_f is that of the thin film signal, and ϕ is the relative phase between substrate (sample holder) and film (sample) third-order nonlinear optical susceptibility.

Explicitly, the signal energy, S_A, at the phase-matched point A, is given by

$$S_A = S_f + \xi^2 S_s + 2\xi(S_f S_s)^{1/2} \cos(\phi_{ijkl}) \qquad (1)$$

where ϕ_{ijkl} is the phase difference and the factor ξ accounts for Fresnel reflection losses (it is a function of thin film and substrate refractive indices; $\xi = 0.843$ for C_{60} on CaF_2). Through comparison of thin film (sample) and substrate (sample holder) measurements, the phase ϕ_{ijkl} can be determined. Since the substrate (sample holder) phase is typically zero (e.g. for fused silica or CaF_2 at visible or near-IR wavelengths) one finds that in the phase-matched signal the superposition of substrate and thin film signals emphasizes the real part of the thin-film third order optical nonlinearity. Therefore, an accurate determination of the real part of the third order optical nonlinearity of a sample can be performed even in the presence of a strongly resonant sample signal. This is in contrast to the Z-scan technique, which is the commonly used technique for phase measurements on solid-state samples.[16] Also, the Z-scan technique is unable to separate thin-film and substrate contributions and is inherently less sensitive than DFWM.

Frequency (wavelength) agility was achieved exploiting computer-controlled optical parametric amplifier (OPA) technology (see next section). As the long wavelength limit of our scans was approached, the phases of all third-order nonlinear optical "Maker−Terhune" tensor components,[17] c_{ijkl}, of the C_{60} sample film approached zero (with respect to the CaF_2 substrate), indicating purely real optical nonlinearity. The magnitude of the $c_{1111}(-\omega,\omega,\omega,-\omega)$ component, governing all parallel polarizations, approaches $10^{-12\pm0.1}$ esu, a factor of 4 smaller than the peak value. Since CaF_2 has a real positive $c_{1111}(0,0,0,0)$ at long wavelengths, so must C_{60}. For comparison, we have also measured $c_{1111}(0,0,0,0)$ for benzene, which is smaller by a factor of 0.03. The Maker−Terhune tensor components are related to the signal energy of the C_{60} film by $S_f = |c_{ijkl}t_f|^2$ where t_f is the sample film thickness.

There are at least eight published theoretical calculations[18] of the long wavelength value, $c_{1111}(0,0,0,0)$, for C_{60} films, all of which are based on a model of C_{60} considered as point dipoles on a fcc lattice whose static moments **m** are related to a local static electric field **e** by the relation

$$\mathbf{m} = \alpha\mathbf{e} + \gamma\mathbf{ee}\cdot\mathbf{e} \qquad (2)$$

The polarizability (α) and second hyperpolarizability (γ) values are related to the refractive index n of the film by the Lorentz−Lorenz relation

$$n^2 = (1 + 8\pi N\alpha/3)/(1 - 4\pi N\alpha/3) \qquad (3)$$

and to the long wavelength limit Maker−Terhune coefficient by

$$c_{1111}(0,0,0,0) = N\gamma L^4/4 \qquad (4)$$

where N is the density of C_{60} ($=1.40 \times 10^{21}$ molecules/cm^3) and L is the Lorentz local-field factor $(n^2 + 2)/3$. Four[19] of the eight calculations predict the observed index of refraction ($=2.0 \pm 0.1$) to within a factor of 2. However, these calculations predict $c_{1111}(0,0,0,0)$ to be from 23 to 76 times smaller than our observed value. Such substantial disagreement between theory and experiment reflects the difficulty of using current quantum mechanical methods for accurately calculating optical and nonlinear properties of condensed phase materials.

Recent measurements of the linear optical absorption in C_{60} films between 1.064 and 1.530 μm give added significance to our $c_{1111}(0,0,0,0)$ measurements.[20] The absorption is less than 2 dB/cm at 1.53 μm. Our measurements suggest that complete optical switching (all-optical signal processing) at the telecommunication wavelength of 1.5 μm can be accomplished without unacceptable optical loss. This can be seen as follows. The self-induced phase change $\Delta\phi$ of an x-polarized plane wave, having traveled a distance d at wave intensity I, is

$$\Delta\phi = 96\pi^3 Id(n^2\lambda c)^{-1} Re[c_{1111}(-\omega,\omega,\omega,-\omega)] \qquad (5)$$

At 1.53 μm and at the nondamaging peak intensities (10^{10} W/cm^2) we use to study C_{60} films, this phase change becomes π radians after 2 mm (one-tenth the absorption length for 2 dB/cm absorption).

It is also appropriate to comment on the peak value of $c_{1111}(-\omega,\omega,\omega,-\omega)$ observed at 0.93 μm. From the following relationship between two-photon absorption coefficient β_2 and the imaginary component of $c_{1111}(-\omega,\omega,\omega,-\omega)$,

$$\beta_2 = 192\pi^3(n^2\lambda c)^{-1} Im[c_{1111}(-\omega,\omega,\omega,-\omega)] \qquad (6)$$

we calculate a β_2 value of 0.02 cm/MW which is equal within experimental error to the peak value of GaAs (at 1.2 μm).[21] Two-photon absorption has a number of technological applications ranging from sensor protection[22] and biomedical imaging[23] (exploiting physical phenomena) to high-density read-only

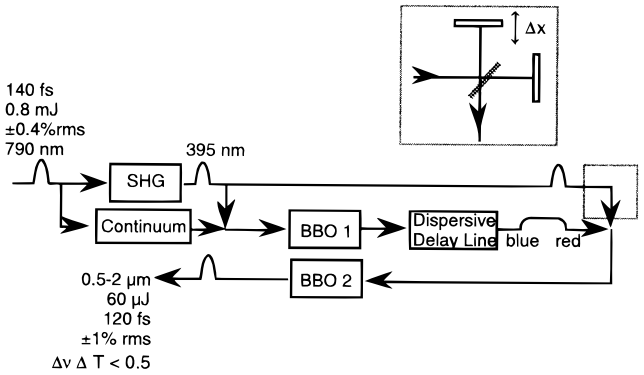

Figure 2. Schematic of our two-stage optical parametric amplifier (OPA) configured for DFWM with typical operating parameters. The inset shows its modification (for nDFWM) to create a double pump−pulse for the second OPA stage which results in a double pulse at the OPA output. The two output pulses are offset in wavelength. The offset is adjusted through the variable delay Δx.

optical memories[24] and polymer cross-linking (exploiting chemical phenomena).[25]

Frequency-Agile DFWM and nDFWM Spectroscopy

As mentioned previously, short femtosecond pulses, pulse stability, frequency-agility, and phase-sensitive-detection are critical to the characterization of "instantaneous" optical nonlinearities such as two-photon absorption. We have already reviewed the realization of phase-sensitive-detection with the signal lattice concept of Figure 1. We have constructed a reliable and ultrastable femtosecond pulse source with performance concerning pulse-to-pulse stability and beam pointing stability that is not currently commercially available.[14] This source is continuously tunable from below 0.5 μm to 2.5 μm (from 0.2 μm to 5 μm with modifications not discussed in this communication) and meets the beam quality requirements of DFWM. The system is based on a highly stable regenerative Ti:sapphire amplifier (1 mJ, $\pm$ 0.4% rms pulse-to-pulse stability at 20 Hz) and a Type I optical parametric amplifier (OPA) which is pumped by the frequency doubled output of the Ti-sapphire amplifier. The OPA delivers over most of its tuning range signal-plus-idler energies near 60 μJ at $\pm$ 1% stability. Type I optical parametric devices suffer from large bandwidth increases in the generated beams near the degeneracy point which is in our case at 0.79 μm. We are able to obtain near transform limited pulses (time bandwidth products of $=$ 0.5) at pulse durations between 100 and 120 fs throughout the tuning range except for an interval of $\pm$ 20 nm which occurs at the degeneracy point. Note that this interval is covered by the tuning range of our Ti:sapphire amplifier. Our optical parametric device is computer controlled which allows access to the full tuning range without manual adjustments.

Our OPA is a two-stage device based on thin, submillimeter thick BBO crystals (schematic diagram shown in Figure 2). It is pumped by a 395 nm femtosecond pulse and seeded by a white light continuum generated through focusing in fused silica. The maximum bandwidth that can be amplified through a parametric process in a given crystal is determined by the effective interaction length: the shorter the interaction length, the broader the generated spectrum. The crystal thickness in our OPA was chosen such that it matches approximately the group-velocity walk-off length, i.e., the length after which one of the participating pulses (signal, idler or pump) has separated from any of the other pulses by more than a pulse width in time. Tuning of the OPA requires adjustment of the tilts of the BBO crystals as well as adjustments of the two pump beam delays relative to the "color" in the continuum beam that one wants to amplify. The bandwidth emerging from the first stage is large. Depending on the center wavelength in our tuning range it can support from less than 10 to about 25 fs pulses. After the first stage, we send the amplified pulse through a dispersive delay line. We find in the second OPA stage that we can, within the bandwidth emerging from the first stage, determine the color of the pulse after the second stage simply by adjusting the second pump−beam delay. Here the wavelength that is amplified is determined by the temporal overlap of the short pump pulse with the "chirped" long pulse arriving from the first stage. The amplification in the second stage is about a factor one hundred such that good discrimination is achieved against the unamplified parts of the bandwidth arriving from the first stage. Under our present operating conditions, tuning the signal wavelength from 0.5 to 0.79 μm requires a delay of the pump of the second stage by about 3 ps. The pulses emerging from our OPA are moderately chirped due to the described generation process. We find from autocorrelation measurements time-bandwidth products of $\leq$ 0.5; i.e., our pulses are still close to transform limited and are thus well suited for DFWM experiments.

An interesting extension of DFWM spectroscopy, namely nearly degenerate four wave mixing (nDFWM), can be implemented by the simple modification of the OPA amplifier shown in Figure 2 (see inset for modification). On the basis of the operational characteristics of our OPA, we use two time-delayed but collinear pump pulses for the second amplification stage. Such a double pulse can be achieved through a "Michelson interferometer" like arrangement as is indicated in the inset of Figure 2. This configuration results in two time- and frequency-separated pulses of about 100 fs duration each. The maximum achievable frequency shift between these pulses varies, depending on center frequency, between 4 to more than 10 pulse bandwidths. We have, for example, tuned our OPA from 0.90 to 1.05 μm simply through the delay of the second-stage pump beam with only minor degradation in output energy. Loss in pump energy of the second OPA stage can be compensated for by appropriate pump collimation optics. The generated double pulse, whose pulses are at frequencies ω and $\omega + \Delta\omega$, is injected into our existing four-wave mixing setup. One of the two pulses can be switched off through use of a shutter in the "Michelson interferometer," if necessary. Depending on the relative delay of the three incident write pulses, we can measure $\chi^{(3)}[-(\omega - \Delta\omega),\omega,\omega,-(\omega + \Delta\omega)]$ and $\chi^{(3)}[-\omega,\omega,\omega,-\omega]$. As usual, the sum of the frequency arguments of $\chi^{(3)}$ is zero; the first of the frequency arguments gives the frequency of the generated signal. Measurements where one records the degenerate and near-degenerate signals in a single computer-controlled run are easily implemented. Comparison of these measurements is facilitated through an already implemented reference branch where a four-wave mixing experiment is performed on a fused silica plate simultaneously with the actual sample measurement. Different cases for write beam and resulting signal beam frequencies based on the beam geometry from Figure 1 are shown in Figure 3. Photon echoes could, in principle, contribute to the observed signals due to the double pulse arrangement. However, this is extremely unlikely and such signals could be observed in single-pulse DFWM experiments (i.e., one pump pulse of the second OPA stage blocked) or through frequency-resolved signal detection (imaging spectrometer with CCD camera) which has already been implemented in our laboratory.

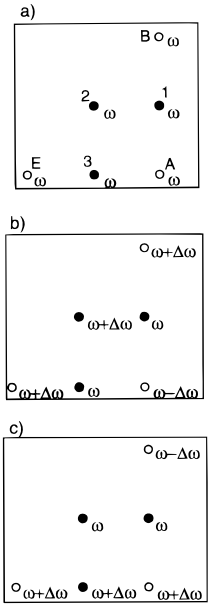

Figure 3. The observation plane of Figure 1 is shown for different frequency configurations of the input beams. The solid dots signify the input beams 1, 2, and 3, the hollow dots signal beams A, B, and E. The beams are also labeled with their frequencies. Configuration 3a corresponds to DFWM while configurations 3b and 3c correspond to nDFWM.

Nearly degenerate four-wave (nDFWM) mixing experiments combine the advantages of THG and DFWM with frequency-shifted signal beams similar to THG but maintaining the "free spectral range" of DFWM for two-photon spectroscopy up $2E_g$. Also, the fact that the gratings in nDFWM are moving limits the effective accumulation time for excited-state gratings to $(\Delta\omega)^{-1}$, the reciprocal of the frequency offset of the grating beams. The shortest effective accumulation times in our implementation of nDFWM are, depending on wavelength, about 5−15 fs. Maximum obtainable frequency shifts result in $h\Delta\omega$ values of about 0.05−0.13 eV. While the THG signal suffers from severe signal reduction due to the large refractive index difference between fundamental and third harmonic, we find in nDFWM only very mild effects of phase mismatch. Under the nDFWM conditions described here, the phase-mismatch-induced signal reduction in thin film samples is negligible. Even in a 1 mm thick fused silica sample we find that phase mismatch effects are very small. For example, if we employ a frequency offset corresponding to 4 times the bandwidth of 100 fs transform limited sech^2 pulses near 0.5 μm in the beam configuration of Figure 3c, we find a signal loss due to phase-mismatch of about 1%.

Besides the improvement in temporal resolution permitting even greater accuracy in the definition of the contributions of excited state absorption and relaxation to measured ("effective") instantaneous optical nonlinearities, a significant but yet unrealized advantage of nDFWM is the characterization of two-photon states lying within the one-photon gap and previously masked by one photon absorptions. To exploit this potential advantage, we have launched a search for the excited A_g state of C_{60}. Realization of the highest frequencies required by such a search requires frequency doubling of our OPA output (to wavelengths as short as 225 nm).

We have also developed a scheme for direct measurement of THG employing a forward DFWM mixing configuration (illustrated in Figure 4). Although the low number of exciting photons available with femtosecond pulses creates some signal-to-noise problems, these are readily overcome by single photon

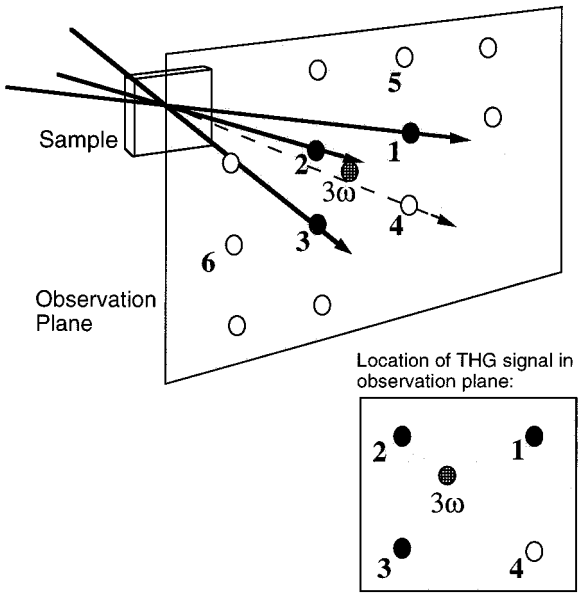

Figure 4. The signal lattice for DFWM-THG is shown. Solid circles show the intersection of write beams with an observation plane. Open circles indicate beams generated by DFWM. The hashed circle indicates the third-harmonic signal generated by beams 1, 2, and 3 consistent with wave vector conservation.

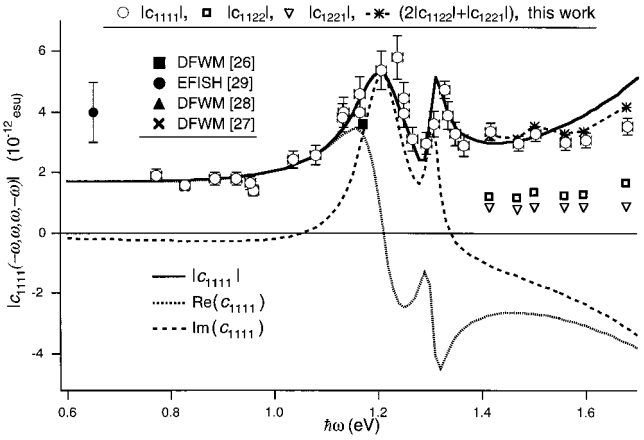

Figure 5. The amplitude (solid line), real (dotted line), and imaginary (dashed line) components of $c_{1111}(-\omega,\omega,\omega,-\omega)$ for C_{70} measured by our femtosecond DFWM techniques (described in the text) are shown. Values of $c_{1122}(-\omega,\omega,\omega,-\omega)$ and $c_{1221}(-\omega,\omega,\omega,-\omega)$ are also shown and indicated by squares and triangles, respectively. These elements are also used to compute $c_{1111}(-\omega,\omega,\omega,-\omega) = 2|c_{1122}(-\omega,\omega,\omega,-\omega)| + |c_{1221}(-\omega,\omega,\omega,-\omega)|$ and compared with direct measurement of that component. Our results are compared with those of others.

counting. The signal lattice detection scheme of Figure 4 also has the advantage of separating contributions from sources other than the thin film sample. The technique has the advantage of permitting explicit investigation of the dependence of $c_{1111}(-3\omega,\omega,\omega,\omega)$ upon pulse width. We denote this technique DFWM-THG.

Application of DFWM Techniques to C_{60} and C_{70}

As nDFWM for C_{60} simply complements the DFWM data discussed above, we will not discuss that data in detail here but rather turn our attention to discussion of results for C_{70}. From various DFWM data (see Figures 5 and 6) collected over a sufficiently large spectral range, together with complementary linear optical susceptibility data, we can calculate all frequency elements of c_{1111} including those associated with

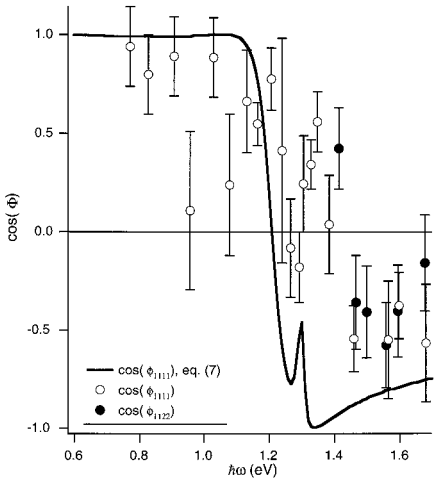

Figure 6. The variation of $\cos(\phi_{1111})$ for C_{70} with spectral energy (frequency) is shown.

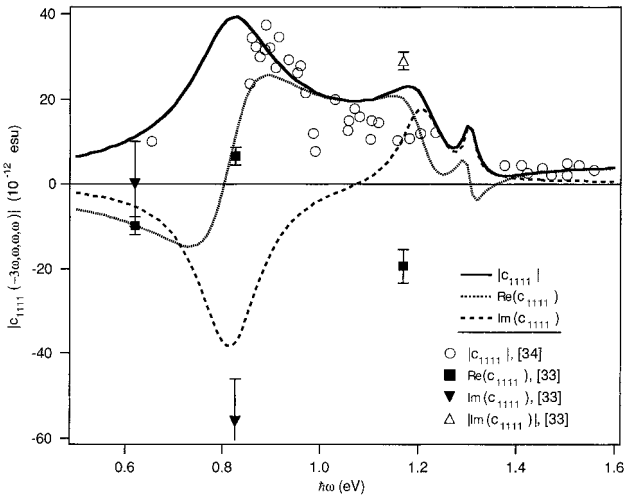

Figure 7. The spectral energy (frequency) dependence of $c_{1111}(-3\omega,\omega,\omega,\omega)$ determined form "DFWM-based" data is shown and compared with conventional THG measurements of others.

THG, $c_{1111}(-3\omega,\omega,\omega,\omega)$, and EFISH, $c_{1111}(-2\omega,\omega,\omega,0)$. Thus, data collected can be compared directly with data collected by THG methods (see Figure 7). We illustrate data collected by our new measurement techniques and the comparison of data obtained by various techniques in Figures 5 and 6.

In Figure 5, we show the magnitude, real, and imaginary components of $c_{1111}(-\omega,\omega,\omega,-\omega)$ for thin films of C_{70} determined in our laboratory by the described femtosecond DFWM techniques (from the data of Figures 5 and 6). We also compare these data with the DFWM and electric-field-induced second-harmonic generation (EFISH) data of others.[26−29] Note that our data permit ready measurement of the symmetry defined splitting (C_{70} is of D_{5h} reduced symmetry compared to the I_h symmetry of C_{60}) of the H_g state of C_{70}. The maxima of the two-photon absorptions associated with the H_g state are observed to occur at 2.61 ± 0.05 and 2.41 ± 0.05 eV. We find the long wavelength limit of $c_{1111}(-\omega,\omega,\omega,-\omega)$ to be 450 times that of fused silica and 1.9 ± 0.6 times that of C_{60}. The nonlinear refractive index (n_2) is, in this limit, $(7.1 \pm 0.8) \times 10^{-14}$ cm^2/W.

In general, all possible states must be considered in the computation of third-order nonlinear optical tensors; however, we have found that it is possible to construct the third-order tensor of C_{70} in the wavelength range of our data from a superposition of three independent terms: (1) A two-state model which contributes a one- and three-photon resonant term, (2) a pure two-photon resonant term, and (3) a nonresonant background term which adds a frequency independent constant to contribution.

The excited state of the two-state model is one-photon allowed and its only excitation pathway is characterized by the sequence of transition dipole moments, $\mu_{\mathbf{ga}}\mu_{\mathbf{ag}}\mu_{\mathbf{ga}}\mu_{\mathbf{ag}}$, where "g" refers to the ground state and "a" to the excited state. For nonmagnetic media, $\mu_{\mathbf{ga}} = \mu_{\mathbf{ag}} = \mu\mathbf{m}$. The contribution to c_{1111} from this term, when the field is along the unit vector $\mathbf{m}$, is completely determined by the linear absorption spectrum in the case where $T_2 \ll T_p \ll T_1$, where T_2 is the transverse relaxation time, T_p is the optical pulse duration, and T_1 is the excited-state lifetime. (A more general discussion based on density matrix theory where the requirement that $T_2 < T_p$ is removed is given elsewhere[5].) From the picosecond DFWM data of Flom et al.,[27] it is clear that $T_1 \gg T_p$, while the absorption spectrum shows that $T_2 \approx T_p/5$. The solution of the Bloch equations for the two-state system gives a real third-order polarization density of the form[30]

$$P_{1P}^{(3)}(t) = -L^4 N\mu \int_{-\infty}^{t} \mathrm{d}t\, \mathrm{e}^{-(t-s)/T_2} w_1(s) \times \sin[\Omega_{1P}(t-s)] \int_{-\infty}^{s} \mathrm{d}u\, \mathrm{e}^{-(s-u)/T_1} w_1(u) \int_{-\infty}^{u} \mathrm{d}v\, \mathrm{e}^{-(u-v)/T_2} w_1(v) \times \cos[\Omega_{1P}(s-v)] \quad (7)$$

where $w_1(t) = -2\mu E(t)/\hbar$ and $\hbar\Omega_{1P}$ is the excitation energy. N is the molecular number density ($=1.2 \times 10^{21}$ molecules/cm^3 for C_{70}). The subscript 1P stands for "one-photon". Again we assume $L = (n^2 + 2)/3$ where we estimate that this may introduce an error of about $\pm 50\%$ in the derived nonlinear polarization density. We use $n = 2.0$ for the linear refractive index of C_{70}. The field $\mathbf{E}(t)$ is a square pulse of duration T_p. We find that it is sufficient to take only the lowest lying absorption line into account to explain our data. The relevant parameters of this line have the following values: $\hbar\Omega_{1P} = 2.45$ eV; $\hbar/T_2 = 0.23$ eV; $\mu = 5.9 \times 10^{-18}$ esu (5.9 D).[31]

We have modeled the two-photon resonances with the Placzek model, which was developed for the analysis of Raman resonances.[32] We demonstrated its applicability to two-photon resonances in the case of C_{60}.[12] It permits calculation of all tensor components c_{ijkl} in contrast to our one-photon resonance model which is presently limited to c_{1111}. The basic assumption of this model is that all the intermediate one-photon states that are connected through a dipole moment to the two-photon state are far from resonance. This is certainly true in the case of DFWM at frequencies below the optical absorption edge but is not necessarily satisfied for THG. The third-order polarization for a single two-photon resonance in this model is given by

$$\vec{P}_{2P}^{(3)}(t) = A\vec{E}(t) \int_{-\infty}^{t} f(t-s)\vec{E}(s)\cdot\vec{E}(s)\, \mathrm{d}s + B \int_{-\infty}^{t} f(t-s)\vec{E}(s)\vec{E}(s)\cdot\vec{E}(t)\, \mathrm{d}s \quad (8)$$

where $f(t) = \sin(\Omega_{2P}t)\exp(-\Gamma t)$. Here the subscript 2P stands for "two-photon"; $\hbar\Omega_{2P}$ is the excited-state energy of the two-photon level and Γ_{2P} its line width. We have fit our DFWM data with a function of the form

$$\vec{P}^{(3)}(t) = \frac{1}{2}\sigma\vec{E}(t)\cdot\vec{E}(t)\vec{E}(t) + \vec{P}_{1P}^{(3)}(t) + \vec{P}_{2P,a}^{(3)}(t) + \vec{P}_{2P,b}^{(3)}(t) \quad (9)$$

that takes 1 one-photon resonance and 2 two-photon resonances (referred to with subscripts "a" and "b") into account. The one-photon resonant term will also give rise to a three-photon resonance as noted earlier. The constant σ represents the

nonresonant background nonlinearity. Even though the resonance peak associated with the lowest one-photon level is outside the wavelength range of our DFWM data, its inclusion into our model is needed to obtain a satisfactory fit. This need is illustrated by the isolated two-photon resonance in C_{60}.[12] In C_{60} the nonlinearity is low on the high-frequency side of the resonance while C_{70} exhibits the opposite behavior. Our best fit gives the following results: $\sigma/8 = 2.2 \pm 0.2 \times 10^{-12}$ esu; $\hbar\Omega_{2P,a} = 2.41 \pm 0.04$ eV, $\hbar\Gamma_{2P,a} = 0.10 \pm 0.01$ eV, $(A + B)_a = 22400$ esu; $\hbar\Omega_{2P,b} = 2.61 \pm 0.04$ eV, $\hbar\Gamma_{2P,b} = 0.025 \pm 0.01$ eV, $(A + B)_b = 33000$ esu. The value $\sigma/8$ represents the nonresonant part of c_{1111} in our frequency range. Due to the negative contributions from the two-level term, we find for the long wavelength limit a value of $1.8 \pm 0.3 \times 10^{-12}$ esu, i.e., smaller than $\sigma/8$. If we use our fit we find the maximum value of two photon absorption (= 0.020 cm/MW). This value is essentially the same as in C_{60} and similar to GaAs, one of the strongest and most studied two-photon absorbers.[21] It is remarkable that in the zero-frequency limit, the one-photon resonant term and the nonresonant term of eq 8 cancel to $0.0 \pm 0.4 \times 10^{-12}$ esu. The sign and magnitude of c_{1111} in that limit is, therefore, determined by the observed two-photon resonances. A similar behavior was found in C_{60}. C_{60} was modeled with only one nonresonant and one two-photon term which yielded $\sigma/8 = -1.4 \pm 0.3 \times 10^{-12}$ esu and $c_{1111}(0,0,0,0) = 0.9 \times 10^{-12}$ esu.[12] The value of $(A + B)$ is a measure for the quadrupole dipole moment products that connect a two-photon state to the ground state. Its value in C_{60} is about 1.7 times larger than that of the larger of the two-photon resonances in C_{70}. From our model, we find that $c_{1111}(0,0,0,0)$ values in both C_{60} and C_{70}, at the telecommunications wavelength of 1.5 microns, are essentially real while the nonlinearity in C_{70} is, at 1.7×10^{-12} esu, about 1.9 times that of C_{60} ($=0.9 \times 10^{-12}$ esu). This allows a pulse propagating in C_{70} at a nondamaging intensity of 10 GW/cm^2 to accumulate a nonlinear phase shift of π after only 1.1 mm of propagation.

Our analysis of $c_{1111}(-\omega,\omega,\omega,-\omega)$ for C_{70} fits a wide range of previously published data obtained through DFWM,[26−28] THG,[33,34] and EFISH.[29] However, due to the use of different reference standards and different definitions of $\chi^{(3)}$, we give here the reference material with their nonresonant reference c_{1111} and their uses: fused silica, 3.95×10^{-15} esu,[14] used for THG and femtosecond DFWM; toluene, 12×10^{-15} esu,[33] used for THG; CS_2, 4.7×10^{-13} esu,[14] used for picosecond DFWM. Due to differing conventions, one often finds values that differ by a factor of 4 or more. We have attempted to correct for different sign conventions in the comparison of data presented here.

Lindle et al.,[26] using 30 ps duration pulses at 1.06 μm, recorded a $c_{1111}(-\omega,\omega,\omega,-\omega)$ value about 5 times higher than the one measured by us, which is not unexpected considering their long pulses which permit nonnegligible excited-state absorption and relaxation. However, if we consider their $c_{1221}(-\omega,\omega,\omega,-\omega)$ value, which is less sensitive to excited-state absorption and relaxation effects, we find better agreement with our measurements (see Figure 5). From et al.[27] performed one-photon resonant picosecond pulse DFWM experiments at 597 and 675 nm. As expected, they find strong excited-state contributions to their measured $\chi^{(3)}$ values. They estimate upper limits for $|c_{1111}(-\omega,\omega,\omega,-\omega)|$ from their $|3\ c_{1221}(-\omega,\omega,\omega,-\omega)|$ values, which are a factor of 5 above our results (see Figure 5). Similarly, Rosker et al.[28] carried out resonant DFWM experiments with femtosecond pulses at 630 nm. Their value is a factor of 4 above our results shown in Figure 5. Unfortunately, they performed their measurement without a reference standard and some sample excitation is contributing to the signal. We thus display their result with a factor of 2 uncertainty.

In Figure 7, we report and compare $c_{1111}(-3\omega,\omega,\omega,\omega)$ data. Our model analysis discussed above relates $c_{1111}(-3\omega,\omega,\omega,\omega)$ and $c_{1111}(-\omega,\omega,\omega,-\omega)$. Let us discuss the comparison of these data with that of others.[29,33,34] Neher et al.[33] have carried out THG measurements on C_{70} dissolved in toluene at 1.17, 0.83, and 0.62 eV. Their measurements yield the real part and the magnitude of the imaginary part of the molecular hyperpolarizability γ_{THG} related to the $c_{1111}(-3\omega,\omega,\omega,\omega)$ value of the thin film by $c_{1111}(-3\omega,\omega,\omega,\omega) = NL^4\ \gamma_{THG}$, where $N = 1.2 \times 10^{21}$ moleucles/cm^3 is the molecular number density in the thin C_{70} film and $L = 2.0$ the corresponding local field factor. Their linear absorption spectrum for a solution sample shows absorption peaks near $\hbar\omega = 2.63$, 3.25, and 3.69 eV which should cause three-photon resonances at $\hbar\omega$ equal to one-third of these values. The corresponding levels in the thin film are found slightly lowered at 2.45, 3.1, and 3.6 eV.[31] As indicated above, our modeling took only the absorption feature at 2.45 eV into account. The THG spectrum near 0.8 eV is dominated by the three photon-resonance associated with this level. The real and imaginary parts of γ_{THG} measured by Neher et al. are in good agreement with our data and modeling (see Figure 7). In particular, we observed a negative real component, $Re[c_{1111}(-3\omega,\omega,\omega,\omega)]$, on the long wavelength side, which is an important signature of the two-state model used by us. Our model assigns a negative sign to $Im(\gamma_{THG})$ at 1.5 μm. The signal measured by Neher et al. is insensitive to small imaginary parts. This explains their measurement of $Im(\gamma_{THG}) = 0$ at 2.0 μm even though its amplitude there is, according to our model, similar to that of $Re(\gamma_{THG})$. Their $|c_{1111}(-3\omega,\omega,\omega,\omega)|$ measured at 1.17 eV is about 7 times higher than that predicted by our model. This is to be expected since we have neglected the two higher energy one-photon transitions.

Wang and Cheng[29] performed EFISH measurements on C_{60} and C_{70} in liquid solution at 1.9 μm. EFISH,[35] such as DFWM, exhibits only one- and two-photon resonances. From their results for C_{70}, we find $c_{1111}(-2\omega,\omega,\omega,0) = 4 \pm 1 \times 10^{-12}$ esu. This is 2.4 times higher than our prediction from DFWM at 1.9 μm (see Figure 5). However, their ratio of the molecular hyperpolarizabilities for C_{70} to C_{60} of 1.7 ± 0.6 is in good agreement with our ratio of 1.9 ± 0.3. It appears therefore that moderate systematic errors are responsible for our disagreement in $|c_{1111}|$.

The THG data measured by Kajzar et al.[34] on thin films appear to be a factor 3 below our values. However, the dependence on energy (frequency) is quite similar to that of our model as can be seen by adjusting the data of Kajzar et al. by a factor of 3. At 0.65 eV, Kajzar et al. report a phase of 0.3 π, which is in contradiction to the result by Neher et al. as well as our model which predicts a phase of 1.2 π. At present we have no explanation for this discrepancy but we notice that the difference in the two results is about π which might be traced back to a sign ambiguity in the data evaluation.

It is clear that, even at a fundamental wavelength of 1.9 microns, THG does not measure the zero frequency limit of the third-order optical nonlinearity while DFWM does so even near 1.2 microns.

In summary, we believe that we have accurately characterized all frequency components of c_{1111} over the wavelength region of our various DFWM measurements, namely, 0.74−2.0 microns. We believe that the model that we have used to achieve a self-consistent fit of our data is also useful for evaluating all

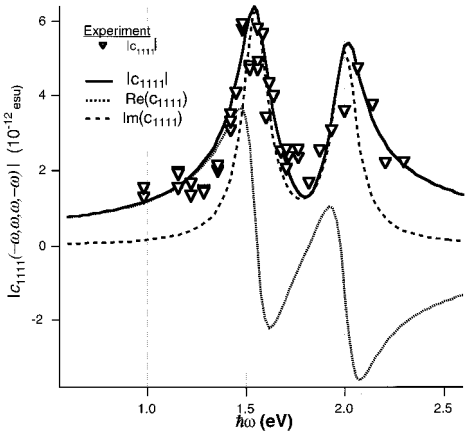

Figure 8. Variation of the amplitude, real, and imaginary components of $c_{1111}(-\omega,\omega,\omega,-\omega)$ for AF-50 with spectral energy (frequency) is shown.

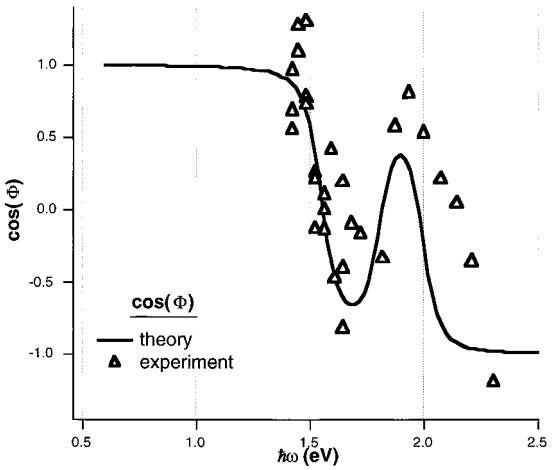

Figure 9. The variation of $\cos(\phi_{1111})$ for AF-50 with spectral energy (frequency) is shown.

current nonlinear spectroscopic data for C_{70}. We have determined the zero frequency limit of c_{1111} for C_{70}, which is 1.9 ± 0.6 times larger than that of C_{60}.

Application to *N*,*N*-Diphenyl-7-[2-(4-pyridinyl)ethenyl]-9,9-di-*n*-decyl-fluoren-2-amine, AF-50

AF-50 is one of a series of two-photon absorbing chromophores prepared by B. A. Reinhardt and co-workers at the Air Force Wright Laboratory.[36] This chromophore was recently reported as having one of the largest two-photon absorption coefficients measured ($\beta_2 = 0.21$ ($\pm$15%) cm/MW for a 0.045 M AF-50/benzene solution at 800 nm wavelength).[36] This is an order of magnitude greater than GaAs. Even more recently, even higher values have been reported for other members of the AF series that have been systematically modified to increase two-photon absorption. However, the fact that the initial measurements were made employing nanosecond pulses raises the question as to the contribution made by excited state absorption to measured ("effective") two-photon absorption coefficients. Also, the initial measurements were made only at selected wavelengths.

We have used the femtosecond DFWM techniques described in this communication to map the real and imaginary components of the third-order optical nonlinearity for wavelengths extending from 575 to 1300 nm for a 0.21 M AF-50/acetone sample contained in a 100 micron thick sample cell. The results are shown in Figures 8 and 9 with theoretical modeling carried out in a manner analogous to that already discussed for the fullerenes. The linear optical spectra of AF-50 in various organic solvents consists of two peaks centered at approximately 320 and 390 nm.[36] The two-photon spectrum that we measure is characterized by two peaks at approximately twice these wavelengths (i.e., 640 and 790 nm). Clearly, the two-photon spectrum mirrors the one-photon spectrum. It is also clear that the measurements made with nanosecond pulses[36] are influenced by excited-state absorption. The instantaneous β_2 value (determined from our DFWM measurements) is less than that of GaAs rather than greater than GaAs as suggested by nanosecond pulse measurements. From our DFWM data, we determine the two-photon absorption cross section, σ_2 of the AF-50 molecule to be 6.7×10^{-21} cm^4/GW, which is a factor of 116 smaller than the value reported in ref 36. Using the relationship $\beta_2 = N\sigma_2$ (where N is again the number density), we calculate a β_2 value of 1.8×10^{-3} cm/MW, about an order of magnitude smaller than the β_2 values GaAs and C_{60}.

Recently, Prasad and co-workers[37] have carried out nonlinear optical (direct optical limiting) measurements employing femtosecond pulses and have determined a β_2 value even smaller (approximately a factor of 5) than that determined from our femtosecond PSD DFWM measurements (Figure 8). We also have recently carried out preliminary direct measurements of optical limiting, using femtosecond pulses, that fall between the recent measurements of Prasad and co-workers and our femtosecond DFWM measurements. Our femtosecond direct optical limiting measurements suggest a value for β_2 a factor of 2 smaller than that determined from femtosecond DFWM. Recently, we have carried out absolute measurements of $Re[c_{1111}(-\omega,\omega,\omega,-\omega)]$ and $Im[c_{1111}(-\omega,\omega,\omega,-\omega)]$ using our femtosecond DFWM techniques; from these measurements, we find a value for β_2 which is a factor of 6 smaller than the value of β_2 determined from our femtosecond DFWM measurements using a reference standard. While the small disagreement between various femtosecond measurements may be insignificant, we nevertheless find it intriguing and plan further investigations to attempt to resolve the issue. It is clear that the data shown in Figure 8 reflect instantaneous two-photon absorption, i.e., the spectral shapes of the resonance are not perturbed by excited-state absorption. This we ascertain from detailed analysis of the temporal characteristics of signals for the different experiments described in this communication. Any disagreement between various measurements must relate to the determination of absolute amplitudes (i.e., the *y*-axis scale of Figure 8) of third-order optical nonlinearities. This, in turn, may relate to the accuracy of values of third-order optical nonlinearity for reference standards used. Another possibility is that the disagreement rests with the accuracy with which we know the exact shape of our femtosecond pulses. Indeed, the fact that we obtain different values of β_2 for experiments using the same instrumental configurations, but differing in the analytical approach (In one case, a reference standard is used, and in the other case, knowledge of the pulse shape is used in an absolute determination) suggests that the basis of the problem may rest with the an inadequate knowledge of pulse shape. Our suspicion, at this time, is that measurements made using a reference standard are more reliable. A third possibility is that pulse-intensity-dependent artifacts come into play reflecting the different magnitudes of pulse intensities used with different measurement techniques. We currently view this possibility the least likely of those discussed. A more detailed analysis our results together with recent femtosecond measurements of Prasad will be published elsewhere.[38]

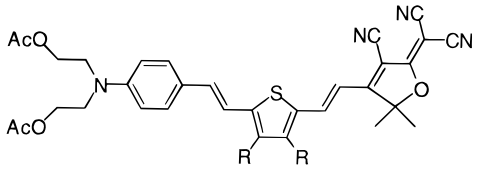

FTC

- μ = 13 D
- $\beta_0 = 635 \times 10^{-30}$ esu (HRS)
- $\mu\beta_{1.9\mu m} = 17{,}600 \times 10^{-48}$ esu (EFISH)
- T_d = 312 °C (DSC, 0 °C/min)
  315 °C (TGA, 10 °C/min)
- λ_{max} = 618 nm in dioxane
  650 nm in $CHCl_3$

Figure 10. The general structure of the FTC chromophore is shown together with optical, second-order nonlinear optical, and thermal data.

In summary, two points are clear from our results for AF-50. The first is that β_2 values clearly depend on pulse width for picosecond and longer pulses, i.e., most systems are going to exhibit excited state absorption and relaxation for these pulse widths. The second is that the AF series is very promising for sensor protection applications as certainly some members of this series can be expected to exhibit two-photon absorption exceeding that of GaAs.

Note that a detailed analysis of two photon absorption has been carried out for AF-50, analogous to that discussed above for the fullerenes. However, since state assignments are not in question for AF50, we omit discussion of that analysis for the sake of brevity.

Application to 2-Dicyanomethylen-3-cyano-4-{2-[*trans*-(4-*N*,*N*-diacetoxyethylamino)phenylene-3,4-dibutylthien-5]-vinyl}-5,5-dimethyl-2,5-dihydrofuran, FTC

The FTC chromophore[39] (structure and relevant optical, nonlinear optical, and thermal data shown in Figure 10) is of interest because of recent use for the fabrication of prototype electrooptic modulators. Steier and Fetterman have used this material to fabricate electrooptic modulators with operating bandwidths considerably greater than 100 GHz.[40] Even at a modest chromophore number density (in various polymer matrixes including high thermal stability hardened polymer lattices) of 1.9×10^{20} molecules/cm^3, this chromophore exhibits the largest recorded electrooptic coefficient (e.g., $r_{33} = 83$ pm/V in poly(methyl methacrylate), PMMA) measured for any device-quality material. A FTC/PMMA film exhibits an optical loss of 0.75 dB/cm at 1.3 microns). Large optical nonlinearity and low optical loss has prompted the use of this material for the development of "optochips" where the polymeric electrooptic circuitry has been successfully integrated with semiconductor VLSI circuitry. A number of technological applications of these materials, ranging from phased array radar to high bandwidth satellite (including Internet) telecommunications are being investigated.

In an effort to fully understand the second and third order nonlinear optical properties of this material, we have carried out measurements of hyper-Rayleigh scattering (HRS), electric-field-induced second-harmonic generation (EFISH), electroabsorption (EA), and femtosecond DFWM. Although extensive measurements have been executed, analysis and modeling are still underway so a more detailed account of this work will be presented elsewhere. However, the preliminary account that we give here provides reasonably accurate determination of several critical parameters of interest to those anticipating use of this or related chromophores. We have executed EFISH measurements[41] at 1.9 microns obtaining a value for $\mu\beta_{1.9\mu m}$ for FTC of 17600×10^{-48}. Hyper-Rayleigh scattering measurements were performed in chloroform (λ_{max} for FTC in $CHCl_3$ is 650 nm), and the known hyperpolarizability of paranitroaniline in this solvent (23×10^{-30} esu)[39,42] was used as a reference. At 1094 nm, the β value for FTC was determined to be 2058×10^{-30} esu. This value is clearly resonant-enhanced and translates into a zero frequency (long wavelength) limit value, β_0, of 635×10^{-30} esu. From EFISH data recorded at 1.9 microns and the measured value of dipole moment ($\mu = 13$ D or 13×10^{-18} esu), we determined $\beta_{1.9\mu m}$ to be 1354×10^{-30} esu. As expected, this value lies between the values at 1.064 microns and the long wavelength limit determined from HRS measurements and modeling. Thus, HRS and EFISH measurements appear to be in reasonable agreement and in agreement with measurements of macroscopic electrooptic coefficients by various techniques.

With T. Treynor and S. Boxer (Stanford University), we have carried out electroabsorption (EA) measurements on frozen (at 77K) 2-methyltetrahydrofuran solutions containing various concentrations of FTC. In these experiments, the change in polarizability with excitation in the presence of an electric field is overwhelmed by the stark effect due to change in dipole upon excitation. We have measured the change in dipole moment and the angle between the dipole-difference and transition-dipole vectors, which is relevant to calculating β from the two state quantum mechanical model. Large intermolecular electrostatic interactions between FTC chromophores appears to lead to chromophore aggregation at high concentrations and low temperatures; this aggregation complicates analysis of EA signals.[39] A detailed account of this work will be published elsewhere.

Femtosecond DFWM measurements of instantaneous optical nonlinearities over the wavelength region from 1 to 1.5 microns suggest a two photon resonance at approximately twice the wavelength of the one-photon interband transition for FTC. This conclusion follows from observation of the variation of both amplitude and phase of $c_{1111}(-\omega,\omega,\omega,-\omega)$ with wavelength, e.g., at 1086 nm, $|c_{1111}(-\omega,\omega,\omega,-\omega)| = 4.0 \times 10^{-13}$ esu, $\phi = 70°$; at 1220 nm, $|c_{1111}(-\omega,\omega,\omega,-\omega)| = 5.4 \times 10^{-13}$ esu, $\phi = 84°$; at 1300 nm, $|c_{1111}(-\omega,\omega,\omega,-\omega)| = 7.2 \times 10^{-13}$ esu, $\phi = 115°$; at 1402 nm, $|c_{1111}(-\omega,\omega,\omega,-\omega)| = 1.1 \times 10^{-12}$ esu, $\phi = 109$; and at 1490 nm, $|c_{1111}(-\omega,\omega,\omega,-\omega)| = 6.7 \times 10^{-13}$ esu, $\phi = 70°$. An analysis of these experimental results, utilizing the theoretical approaches discussed previously, is shown in Figure 11. Our measurements and analysis for FTC/PMMA again illustrate the importance of measuring phase as well as amplitude in DFWM experiments. The unusual spectral shape of $c_{1111}(-\omega,\omega,\omega,-\omega)$ likely reflects the contribution of an additional mechanism (possibly a second two-photon peak which might be associated with isolated FTC molecules or with FTC dimers). Another possibility is that the electron density on the donor portion of the FTC molecule is sensitive to hydrogen bonding involving the amine nitrogen. Such hydrogen bonding could be a problem if the protecting groups (Ac) are removed inadvertently.

At 1.3 microns and for a 15% (wt/wt) FTC/PMMA thin film sample, we determined $|c_{1111}(-\omega,\omega,\omega,-\omega)| = 7.2 \times 10^{-13}$ esu which can be used to calculate a β_2 value of 3.8×10^{-3} cm/MW (assuming that there are not other contributions to $c_{1111}(-\omega,\omega,\omega,-\omega)$ at 1.3 μm which may obviously not be correct). While it is not unreasonable that FTC and AF-50 exhibit comparable two-photon absorption coefficients, specification of

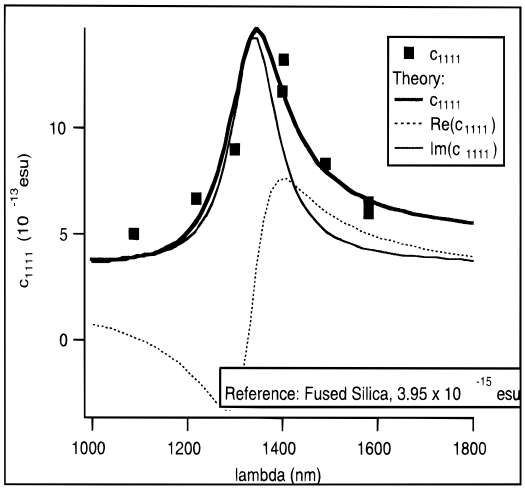

Figure 11. Experimental data and theoretical analysis of that data are provided for the FTC chromophore as described in the text.

more precise magnitudes of β_2 for these materials must await further measurements and more detailed analysis. However, the existence of a two photon resonance near telecommunication wavelengths is important information for those anticipating use of the FTC chromophore for electrooptic device applications. The large values of β_2 at 1.3 and 1.5 microns, together with modest optical loss at these wavelengths, suggests the potential for use of FTC-like chromophores in all-optical switching applications, but concern must exist for two photon induced photochemistry.

Characterization of Excited-State Absorption and Relaxation

To understand the behavior of materials in devices such as optical limiters, optical switches, and electrooptic modulators, one must in general have a thorough understanding of a variety excited state absorption and relaxation processes. For example, thermal processes can have dramatic effects on device performance. In like manner, the behavior of photoactive biological materials can be influenced by a variety of effects. For example, eye damage from continuous wave radiation and light pulses of nanosecond duration or longer is dominated by thermal effects. If picosecond pulses are employed, photoacoustic, structural relaxation, and electronic effects may come into play and must be explicitly considered to define meaningful damage (sensor protection) thresholds. Femtosecond pulses will likely come into play only through photochemical damage processes involving the electronic structure of the chromophore. Of particular relevance to the present work is the fact that two photon absorption can lead to thermal heating and to chemical reactions. By design, these events can be exploited to advantage in the development of hybrid sensor protection elements where two-photon absorption leads to ultrafast but moderate optical limiting while thermal and chemical effects lead to slow but large optical limiting effects.

To understand a wide range of dynamical effects, detailed analysis of time-dependent signals over several decades of time is typically required. For experiments where pulses periods are significantly greater than phase relaxation times of the material, analysis of temporal phenomena can be effected using a Bloch equation approach, i.e., considering only state population evolution. However, more general analysis typically requires a density matrix approach which considers both phase and population relaxation in the material system and explicitly considers the details of the time-dependent applied radiation.[5,13] A density matrix stochastic Liouville approach permits both quantum mechanic and classical aspects of the evolution of a system (after pulsed excitation) to be treated; we have, for example, explicitly treated classical thermal diffusion and photoacoustic effects via the density matrix-stochastic Liouville approach.[13]

We have carried out investigation of the materials discussed here over time scales extending from the femtosecond to nanosecond time scales with detailed temporal analysis carried out as discussed above. For the sake of brevity, we omit a detailed discussion of this work and only indicate that analysis supports the contention that sub-100 fs measurements reflect instantaneous optical nonlinearities while picosecond and longer measurements are significantly influenced by excited-state absorption and relaxation.

Conclusions

Femtosecond DFWM techniques executed with phase-sensitive detection and wavelength agility over the spectral range 0.45 to 2.5 microns are effective tools for characterizing instantaneous optical nonlinearities. We have characterized the lowest lying two photon absorptions for C_{60}, C_{70}, and AF-50 and carried out a preliminary measurement of two-photon absorption in the chromophore FTC. Instantaneous two-photon absorption coefficients for the fullerenes and the AF series of chromophores are clearly competitive with GaAs. Our measurements demonstrate that all of these materials exhibit excited-state absorption and relaxation that cause two-photon absorption coefficient measurements carried out using longer (pico- and nanosecond) pulses to yield larger values which must be viewed as "effective" or pulse width-dependent two-photon absorption coefficients. DFWM techniques are also shown to exhibit the advantage, relative to THG, of avoiding the overlap of two-photon absorptions with one and three photon absorptions. This has proven to be critical for correctly assigning the lowest lying H_g two-photon state of the fullerenes. These results, like those of Kohler for polyenes, are crucial for testing quantum mechanical theories.

The studies reported here are useful for understanding some of the current limits to highly accurate measurement of absolute values of third order optical nonlinearities (i.e., nonlinear absorption and index of refraction). The importance of accurate definition of optical nonlinearity of reference standards and of pulse shapes for direct absolute measurements is emphasized by the studies reported here. It is also clear that the details of each measurement technique must be carefully considered to avoid artifacts and minimize measurement errors.

In addition to providing improved characterization of instantaneous optical nonlinearities, new DFWM techniques are useful for characterizing excited-state absorption processes through analysis of the temporal response over many orders of magnitude of time and over a significant range of wavelengths. Meaningful extraction of data in general requires density matrix analysis explicitly considering both phase and population analysis and the details of applied pulses and the detection scheme. Satisfactory analysis can require the consideration of thermal, photoacoustic, translational diffusion, and rotational diffusion effects as well as electronic effects. Detailed characterization of complex condensed phase materials can necessitate the use of complementary measurements and quantum mechanical calculations to assign states participating in the evolution of optical excitation.

Our measurements of optical nonlinearities for the fullerenes, AF-50, and FTC indicate the potential of these materials for

use as device materials. FTC clearly can be used in electrooptic device configurations such as Mach−Zender modulators, birefringent modulators, and directional couplers. The two photon absorption observed for FTC raises some concern for photochemical reactions having some effect on the operation of devices fabricated from this material. However, analysis of the temporal behavior over longer time periods for samples exposed to pulsed radiation does not suggest problematic photochemical processes. The fullerenes and the AF series have potential for use as optical limiters and all-optical switches particularly if the intrinsic material optical nonlinearity is enhanced through nanoscale architectures such as light harvesting dendrimers or photonic band gap structures.

Acknowledgment. We gratefully acknowledge the support of this work by the National Science Foundation (Grant DMR-9528021) and by the U.S. Air Force Office of Scientific Research (Grants F49620-95-1-0450, F49620-96-1-0035, and F49620-97-1-0307). We are indebted to the following individuals for invaluable assistance: Drs. C. Y-C. Lee, R. W. Hellwarth, H. W. Kafafi, P. N. Prasad, P. Fleitz, B. A. Reinhardt, A. Persoons, J. Zyss, T. Treynor, S. Boxer, and A. W. Harper.

References and Notes

(1) Hudson, B. S.; Kohler, B. E. *Chem. Phys. Lett.* **1972**, *14*, 299. Christensen, R. L.; Kohler, B. E. *J. Chem. Phys.* **1975**, *63*, 1837. Granville, M. F.; Holtom, G. R.; Kohler, B. E. *J. Chem. Phys.* **1980**, *72*, 4671. Auerbach, R. A.; Christensen, R. L.; Granville, M. F.; Kohler, B. E. *J. Chem. Phys.* **1981**, *74*, 4. Hudson, B. S.; Kohler, B. E.; Schulten, K. *Excited States* **1981**, *6*, 1. Hudson, B. S.; Kohler, B. E. *Synth. Met.* **1984**, *53*, 241. Kohler, B. E. *Springer Ser. Solid-State Sci.* **1985**, *63*, 100. Horwitz, J. S.; Kohler, B. E.; Spiglanin, T. A. *J. Phys. Colloq.* **1985**, 381. Horwitz, J. S.; Itoh, T.; Kohler, B. E.; Spangler, C. W. J. *Chem. Phys.* **1987**, *87*, 2433. Kohler, B. E. *J. Chem. Phys.* **1988**, *88*, 2788. Kohler, B. E.; Spangler, C. W.; Westerfield, C. *J. Chem. Phys.* **1988**, *89*, 5422. Kohler, B. E.; Itoh, T. *J. Phys. Chem.* **1988**, *92*, 5120. Kohler, B. E. *Mater. Res. Soc. Symp. Proc.* **1990**, *173*, 649. Kohler, B. E. *J. Chem. Phys.* **1990**, *93*, 5838. Buma, W. J.; Kohler, B. E.; Song, K.; *J. Chem. Phys.* **1990**, *92*, 4622. Aoyagi, M.; Ohmine, I.; Kohler, B. E. *J. Phys. Chem.* **1990**, *94*, 3922. Kohler, B. E. *Conjugated Polym.* **1991**, 405. Kohler, B. E. *Synth. Met.* **1991**, *41*, 1215. Dauben, W. G.; Disanayaka, B.; Funhoff, D. J. H.; Zhou, B.; Kohler, B. E.; Schilke, D. E. *J. Am. Chem. Soc.* **1991**, *113*, 8367. Kohler, B. E.; Spangler, C. W.; Westerfield, C. *J. Chem. Phys.* **1991**, *94*, 908. Birbaum, D.; Fichou, D.; Kohler, B. E. *J. Chem. Phys.* **1992**, *96*, 165.

(2) Service, R. *Science* **1995**, *267*, 1918. Nalwa, S. W.; Miyata, S. *Nonlinear Optics of Organic Molecules and Polymers*; CRC Press: Boca Raton, 1997. Wise, D. L.; Wnek, G. E.; Trantolo, D. J.; Cooper, T. M.; Gresser, J. D. *Electrical and Optical Polymer Systems*; Marcel Dekker: New York, 1998. Prasad, P. N.; Williams, D. J. *Introduction to Nonlinear Optical Effects in Molecules and Polymers*; Wiley: New York, 1991. Dalton, L. R. Nonlinear optical materials. In *Kirk-Othmer Encyclopedia of Chemical Technology*, 4th ed.; Wiley-Interscience: New York, 1996, Vol. 17, p 287. Reynolds, J. R.; Jen, A. K. Y.; Rubner, M. F.; Chiang, L. Y.; Dalton, L. R. *Electrical, Optical, and Magnetic Properties of Organic Solid-State Materials IV*; Materials Research Society: Pittsburgh, 1998; Vol. 488. Jenekhe, S. A.; Wynne, K. J. *Photonics and Optoelectronic Polymers*; ACS Symposium Series 672; American Chemical Society: Washington, DC, 1997. Dalton, L. R.; Harper, A. W.; Wu, B.; Ghosn, R.; Laquinadanum, J.; Liang, Z.; Hubbel, A.; Xu, C. *Adv. Mater.* **1995**, *7*, 519; Dalton, L. R.; Sapochak, L. S.; Chen, M.; Yu, L. P. Ultrastructure concepts of optical integrated microcircuits and polymeric materials. In *Molecular Electronics and Molecular Electronic Devices*; Sienicki, K., ed.; CRC Press: Boca Raton, FL, 1993; p 125. Dalton, L. R.; Harper, A. W. *Polym. News* **1998**, *23*, 114. Burroughes, J. H.; Bradley, D. D. C.; Brown, A. R.; Marks, R. N.; Mackay, K.; Friend, R. H.; Burns, P. L.; Holmes, A. B. *Nature (London)* **1990**, *347*, 1990; Braun, D.; Heeger, A. J. *Appl. Phys. Lett.* **1991**, *58*, 1982. Moerner, W. E.; Silence, S. M.; Hache, F.; Bjorklund, G. C. *J. Opt. Soc. Am. B* **1994**, *11*, 320. Moerner, W. E.; Silence, S. M. *Chem. Rev.* **1994**, *94*, 127. Tang, C. W.; Van Slyke, S. A.; Chen, C. H. *J. Appl. Phys.* **1989**, *65*, 3610. Tutt, L. W.; Boggess, T. F. *Prog. Quantum Electron.* **1993**, *17*, 299. Van Stryland, E. W.; Vanherzeele, H.; Woodall, M. A.; Soileau, M. J.; Smirl, A. L.; Gurha, S.; Boggess, T. F. *Opt. Eng.* **1985**, *24*, 613. Ehrich, J. E.; Wu, X. L.; Lee, I. Y. S.; Hu, Z. Y.; Marder, S. R.; Perry, J. W. *Opt. Lett.* **1997**, *22*, 1843. He, G. S.; Bhawalkar, J. D.; Zhao, C. F.; Prasad, P. N. *Appl. Phys. Lett.* **1995**, *67*, 2433.

(3) Birge, R. R. *Sci. Am.* **1995**, *272*, 90. Chen, Z.; Govender, D.; Gross, R.; Birge, R. R. *BioSystems* **1995**, *35*, 145. Birge, R. R.; Gross, R. B.; Lawrence, A. F. *Mol. Electron.* **1996**, 333. Talent, J.; Song, Q. W.; Li, J.; Stuary, J.; Birge, R. R. *Opt. Lett.* **1996**, *21*, 1339. Birge, R. R. In Proceedings of Nanotechnology for the Soldier System Conference, Boston, July 7−9, 1998.

(4) Boyd, R. W. *Nonlinear Optics*; Academic: San Diego, 1992. Bloembergen, N. *Nonlinear Optics*; Benjamin, New York, 1965. Prasad, P. N.; Williams, D. J. *Introduction to Nonlinear Optical Effects in Molecules and Polymers*; Wiley: New York, 1991. Dalton, L. R. Nonlinear optical materials. In *Kirk-Othmer Encyclopedia of Chemical Technology*, 4th ed.; Wiley-Interscience: New York, 1996; Vol. 17, p 287. Bain, A. N.; Yu, L. P.; Chen, M.; Sapochak, L. S.; Dalton, L. R. *Spectrosc. Int. J.* **1990**, *8*, 73.

(5) Dalton, L. R.; Sapochak, L. S.; Yu, L. P. *J. Phys. Chem.* **1993**, *97*, 2871.

(6) Brady, B. B.; Beiting, E. J. *J. Chem. Phys.* **1992**, 97, 1992. Leach, S.; Vervloet, M.; Despres, A.; Breheret, E.; Hare, J. P.; Dennis, T. J.; Kroto, H. W.; Taylor, R.; Walton, D. R. M. *Chem. Phys.* **1992**, *160*, 451. Kajzar, F.; Taliani, C.; Zamboni, R.; Rossini, S.; Danieli, R. *Synth. Met.* **1993**, *54*, 21.

(7) Weaver, J. H.; Martins, J. L.; Komeda, T.; Chen, Y.; Ohno, T. R.; Kroll, G. H.; Troullier, N.; Haufler, R. E.; Smalley, R. E. *Phys. Rev. Lett.* **1991**, *66*, 1741.

(8) Hung, R. R.; Grabowski, J. J. *J. Phys. Chem.* **1991**, *95*, 6073. Zeng, Y.; Biczok, L.; Linschitz, H. *J. Phys. Chem.* **1992**, *96*, 5237.

(9) Negri, F.; Orlandi, G.; Zerbetto, F. *Chem. Phys. Lett.* **1992**, *144*, 31.

(10) Laxzlo, I.; Udvardi, L. *J. Mol. Struct.* **1989**, *183*, 271.

(11) Kajzar, F.; Taliani, C.; Zamboni, R.; Rossini, S.; Danieli, R. *Synth. Met.* **1993**, *54*, 21. Meth, J. S.; Vanherzeele, H.; Wang, Y. *Chem. Phys. Lett.* **1992**, *197*, 26. Kajzar, F.; Taliani, C.; Danieli, R.; Rossini, S.; Zamboni, R. *Chem. Phys. Lett.* **1994**, *217*, 418.

(12) Strohkendl, F. P.; Axenson, T. J.; Larsen, R. J.; Dalton, L. R.; Hellwarth, R. W.; Kafafi, Z. H. *J. Phys. Chem. B* **1997**, *101*, 8802.

(13) Bain, A. N.; Yu, L. P.; Chen, M.; Sapochak, L. S.; Dalton, L. R. *Spectrosc. Int. J.* **1990**, *8*, 73.

(14) Strohkendl, F. P.; Files, D. J.; Dalton, L. R. *J. Opt. Soc. Am. B* **1994**, *11*, 742; Strohkendl, F. P.; Dalton, L. R.; Hellwarth, R. W.; Sarkas, H. W.; Kafafi, Z. H. *J. Opt. Soc. Am.* B. **1997**, *14*, 92. Strohkendl, F. P.; Axenson, T. J.; Dalton, L. R.; Hellwarth, R. W.; Sarkas, H. W.; Kafafi, Z. H. *Proc. SPIE* **1996**, *2854*, 191. Strohkendl, F. P.; Axenson, T. J.; Larsen, R. J.; Dalton, L. R.; Hellwarth, R. W.; Kafafi, Z. H. *Proc. SPIE* **1997**, *3142*, 2.

(15) Banfi, G. P.; Fortusini, D.; Bellini, M.; Miliani, P. *Phys. Rev. B* **1997**, *56*, 10075.

(16) Sheik-bahae, M.; Said, A. A.; Van Stryland, E. W. *Opt. Lett.***1989**, *14*, 955. Sheik-bahae, M.; Hutchings, D. C.; Hagan, D. J.; Van Stryland, E. W. *IEEE J. Quantum Electron.* **1991**, *27*, 1296.

(17) Maker, P. D.; Terhune, R. W. *Phys. Rev.* **1965**, *137*, A801. The $c_{ijkl}(-\omega,\omega,\omega,-\omega)$ coefficients are often called $\chi_{ijkl}(-\omega,\omega,\omega,-\omega)$. However, the latter appear with many different (implied) factors in the literature, depending on whether complex field amplitudes or Fourier amplitudes are used, and on several other conventions.

(18) Rustagi, K. C.; Ramaniah, L. M.; Nair, S. V. *Int. J. Mod. Phys. B* **1992**, *6*, 3941. Shuai, Z.; Bredas, J. L. *Phys. Rev. B* **1992**, *46*, 16135. Li, J.; Feng, J.; Sun, J. *Chem. Phys. Lett.* **1993**, *203*, 560. Knize, R. J. *Opt. Commun.* **1994**, *106*, 95. Quong, A. A.; Pederson, M. R. *Phys. Rev. B* **1992**, *46*, 12906. Williame, F.; Falicou, L. M. *J. Chem. Phys.* **1993**, *98*, 3941. Wang, Y.; Bertsch, G. F.; Tomanek, D. Z. *Phys. D* **1993**, *25*, 181. Westin, E.; Rosen, A. *Appl. Phys. A* **1995**, *60*, 49.

(19) Quong, A. A.; Pederson, M. R. *Phys. Rev. B* **1992**, *46*, 12906. Williame, F.; Falicou, L. M. *J. Chem. Phys.* **1993**, *98*, 3941. Wang, Y.; Bertsch, G. F.; Tomanek, D. Z. *Phys. D* **1993**, *25*, 181. Westin, E.; Rosen, A. *Appl. Phys. A* **1995**, *60*, 49.

(20) Jager, M.; Zhang, Q.; Stegeman, G. I.; Merritt, C. D.; Kafafi, Z. H. *Proc. Am. Chem. Soc. Div. Polym. Mater.: Sci. Eng.* **1996**, 222.

(21) Van Stryland, E. W.; Chase, L. L. *CRD Laser Handbook of Laser Science and Technology, Supplement 2*; Weber, M. J., Ed.; CRC Press: Boca Raton, FL., 1995; p 299.

(22) Ralston, J. M.; Chang, K. R. *Appl. Phys. Lett.* **1969**, *15*, 164.

(23) Denk, W.; Strickler, J. H.; Webb, W. W. *Science* **1990**, *248*, 73. Denk, W.; Delaney, K. R.; Gelperin, A.; Kleinfeld, D.; Strowlridge, B. W.; Tank, D. W.; Yuste, R. *J. Neurosci. Methods* **1994**, *54*, 151. Hell, S. W.; Hanninen, P. E.; Kuusisto, A.; Schrader, M.; Soini, E. *Opt. Commun.* **1995**, *117*, 20.

(24) Parthenopoulos, D. A.; Rentzepis, P. M. *Science* **1989**, *245*, 843. Dvornikov, A. S.; Cokgor, I.; McCormick, F.; Piyaket, R.; Esener, S.; Rentzepis, P. M. *Opt. Commun.* **1996**, *128*, 205. Piyaket, R.; Cokgor, A. S.; McCormick, F. B.; Esener, S.; Dvornikov, A. S.; Rentzepis *Opt. Lett.* **1996**, *21*, 1032.

(25) Strickler, J.; Webb, W. W. *Opt. Lett.* **1991**, *16*, 1780. Ehrlich J. *OSA Technol. Digest Ser.* **1997**, *14*, 64.

(26) Lindle, J. R.; Pong, P. G. S.; Bartoli, F. J.; Kafafi, Z. H. *Phys. Rev. B* **1993**, *48*, 9447.

(27) Flom, S. R.; Pong, R. G. S.; Bartoli, F. J.; Kafafi, Z. H. *Phys. Rev. B* **1992**, *46*, 15598.

(28) Rosker, M. J.; Marcy, H. O.; Chang, T. Y. *Chem. Phys. Lett.* **1992**, *196*, 427.

(29) Wang, Y.; Cheng, L. T. *J. Phys. Chem.* **1992**, *96*, 1530.

(30) For a more detailed discussion of Bloch and density matrix calculations, see: refs 5 and 13.

(31) Ren, S. L.; Zhou, P.; Wang, Y.; Rao, A. M.; Meier, M. S.; Selegue, J. P.; Eklund, P. C. *Appl. Phys. Lett.* **1992**, *61*, 124.

(32) Placzek, G. *The Rayleigh and Raman Scattering*; US. Department of Commerce: Washington, DC, 1962 (UCRL Translation 256 (L)).

(33) Neher, D.; Stegeman, G. I.; Tinker, F. A.; Peyghambarian, N. *Opt. Lett.* **1992**, *17*, 1491.

(34) Kajzar, F.; Taliani, C.; Danieli, R.; Rossini, S.; Zamboni, R. *Phys. Rev. Lett.* **1994**, *73*, 418.

(35) For EFISH and DFWM, $c_{1111} = c_{1221} + c_{1122}$, while for THG, $c_{1111} = 3\ c_{1212}$. In the long wavelength limit and for isotropic media, c_{1122}, c_{1221}, and c_{1212} become equal.

(36) He, G. S.; Yuan, L.; Cheng, N.; Bhawalkar, J. D.; Prasad, P. N.; Brott, L. L.; Clarson, S. J.; Reinhardt, B. A. *J. Opt. Soc. Am. B* **1997**, *14*, 1079.

(37) Prasad, P. N. Private communication.

(38) Prasad, P. N.; Reinhardt, B. A.; Fleitz, P.; L. R. Dalton; Strohkendl, F. P.; Larsen, R. J.; Drenser, K. A. Unpublished data.

(39) Wang, F. Ph.D. Dissertation, University of Southern California, Los Angeles, CA, 1998. Chen, A. Ph.D. Dissertation, University of Southern California, Los Angeles, CA, 1998. Dalton, L. R. and co-workers. Unpublished data.

(40) Fetterman, H. R. Proc. IEEE/LEOS Conference, Monterey, CA, July, 1998. Steier, W. H. Proceedings of the IEEE/LEOS Conference, Monterey, CA, July, 1998.

(41) Dalton, L. R.; Harper, A. W.; Ghosn, R.; Steier, W. H.; Ziari, M.; Fetterman, H.; Shi, Y.; Mustacich, R. V.; Jen, A. K. Y.; Shea, K. J. *Chem. Mater.* **1995**, *7*, 1060.

(42) Clays, K.; Persoons, A. *Rev. Sci. Instrum.* **1992**, *63*, 3285. Persoons, A.; Houbrechts, S.; Wang, F.; Dalton, L. R. Unpublished data to be published.

(43) There are fortunately important exceptions to this statement including Kerr effect Ti:sapphire used for high stability mode-locked pico- and femtosecond lasers and BBO used for OPO/OPA applications as described in this manuscript.